JOURNAL OF CATALYSIS 92, 216–231 (1985)

Selective Oxidation of n-Butane to Maleic Anhydride by Model V–P–O Catalysts

T. P. MOSER AND G. L. SCHRADER[1]

Department of Chemical Engineering and Ames Laboratory—USDOE, Iowa State University, Ames, Iowa 50011

Received June 20, 1984; revised November 23, 1984

The selective oxidation of n-butane to maleic anhydride was studied using two model vanadium–phosphorus–oxygen catalysts, β-$VOPO_4$ and $(VO)_2P_2O_7$. Detailed information concerning the synthesis and characterization of these phases was developed, which indicated the sensitivity of the syntheses to preparation procedures. New information regarding the possible reaction pathway was provided by the detection of 1-butene, 2-butenes, and 1,3-butadiene simultaneously with the production of maleic anhydride. The stability of the pure phases under reaction conditions was examined using *in situ* laser Raman spectroscopy. © 1985 Academic Press, Inc.

1. INTRODUCTION

To a significant extent, industrial processes for producing partially oxidized hydrocarbons by heterogeneous catalysis have previously relied on olefinic and aromatic hydrocarbon feedstocks. Ethylene and propylene are used in the dominant routes to ethylene oxide and acrylonitrile, respectively. Aromatics such as benzene and naphthalene can be converted to anhydrides through high-temperature selective oxidation catalysis. Methanol oxidation is also an important industrial route for producing formaldehyde, a valuable industrial chemical. In contrast, heterogeneous catalytic synthesis involving the selective oxidation of paraffins currently represent only a small portion of the total output of chemicals and intermediates in the United States; rapid growth of this processing technology has been predicted, however (*1*).

The major industrial route for producing maleic anhydride in the United States currently uses benzene as the hydrocarbon feedstock. The oxidation of n-butane has also been practiced for several years now, constituting about 15% of the total output of maleic anhydride (*2*). The reliance on the paraffin feedstock is expected to increase significantly as benzene becomes more expensive and difficult to use, due in part to environmental restrictions.

Several investigations have been reported in the recent literature which deal with the catalytic chemistry of n-butane conversion to maleic anhydride using vanadium–phosphorus–oxygen (V–P–O) catalysts. The most relevant aspects of this previous work for our current investigations have been the identification and evaluation of various catalytically active V–P–O phases and the suggestion of various reaction pathways for n-butane oxidation. A brief summary of the current status of the literature follows.

Efforts to develop active, selective, and stable catalysts for n-butane oxidation have been clearly revealed in the patent literature (*3*). The most widely claimed catalyst composition is based on vanadium, phosphorus, and oxygen; catalyst modifiers include iron, molybdenum, chromium, cobalt, nickel, zirconium, zinc, copper, and several other metals. Specific V–P–O cata-

[1] To whom correspondence should be addressed.

0021-9517/85 $3.00

lyst phases have been examined because of their apparent relevance for n-butane oxidation. A significant portion of our work has been concerned with the synthesis and characterization of these phases.

The existence of β-$VOPO_4$ was first reported by Brown and Hummel (*4*), and structural information has been provided by several researchers (*5–7*). Vibrational spectroscopic characterization has also been reported (*5, 8*). Higher purity β-$VOPO_4$ can apparently be prepared by solid-state synthesis (*5–8*); preparation by precipitation or by evaporation to dryness has also been reported (*5, 9–12*). Hodnett *et al.* (*9*) investigated catalysts with various P/V ratios, and catalysts with low phosphorus loadings (P/V = 0.94) had X-ray *d*-spacings characteristic of the β-$VOPO_4$ phase. Although low selectivity was reported for this composition, catalysts with P/V = 0.97 were highly selective for n-butane conversion to maleic anhydride.

The crystal structure of another phase, $(VO)_2P_2O_7$, was examined by Bordes and Courtine (*5*); they also reported the infrared spectrum of this compound. The kinetics of n-butane oxidation using $(VO)_2P_2O_7$ was studied by Wüstneck *et al.* (13); the activity of an additional phase, α-$VOPO_4$, was also investigated by these researchers.

A greater number of studies involving catalytic materials with various P/V ratios have been reported, although these systems probably do not have single-phase compositions (*9, 12, 14, 15*). Many of these studies have also involved 1-butene oxidation rather than n-butane oxidation.

Kinetics and mechanism studies of n-butane oxidation have been relatively few in number. A three-step reaction pathway has been proposed by Wohlfahrt and Hofmann (*16*) and Escardino *et al.* (*17*). For this proposal, n-butane is converted to maleic anhydride or to CO, CO_2, and H_2O. Maleic anhydride can also be combusted to the latter products. No observation of the presence of 1-butene, 2-butenes, or 1,3-butadiene has been reported in the current literature for reactors operated at high temperatures with low concentrations of hydrocarbons in the feed (lean mixtures).

Successful and reproducible syntheses of two V–P–O phases (β-$VOPO_4$ and $(VO)_2P_2O_7$) are reported in this paper. We also provide extensive characterization of these phases. The activity and selectivity of β-$VOPO_4$ and $(VO)_2P_2O_7$ for n-butane oxidation are presented. The observation of C_4 olefinic products is also reported. The stability of the pure phases under reaction conditions has also been established using *in situ* laser Raman spectroscopy.

2. EXPERIMENTAL PROCEDURE

2.A. Syntheses of Model V–P–O Catalysts

2.A.1. β-$VOPO_4$. The β-$VOPO_4$ phase was prepared by solid-state reaction of $NH_4H_2PO_4$ and V_2O_5. The solid precursors were powdered, mixed, and ground together in the appropriate stoichiometric proportion (P/V = 1.00). The mixture was then transferred to either a quartz crucible or a platinum-foil-lined quartz crucible and calcined under a flow of dry oxygen (dried with silica gel) at 200°C for 4 h. The reacted material was removed from the furnace, homogenized by grinding, and then reinserted into the furnace. The temperature was stepped to 400°C for 4 h; the furnace temperature was then held at 600°C for 12 h. A cooling rate of 40°C per hour or less was found to be critical in obtaining a material which was free of polycondensed phosphates. The resulting β-$VOPO_4$ crystals were yellow–green in color and had a surface area of 1.90 m^2/g.

2.A.2. $(VO)_2P_2O_7$. The $(VO)_2P_2O_7$ phase was prepared by solid-state reaction of $NH_4H_2PO_4$ and V_2O_5. The solid precursors were powdered, mixed, and ground together in the appropriate stoichiometric proportion (P/V = 1.00). The mixture was calcined under dry oxygen (dried by silica gel) in a quartz crucible at 200°C for 4 h.

This intermediate synthesis material was removed from the furnace and homogenized by grinding in an agate mortar. Calcination was resumed at 400°C with a steady flow of oxygen for four hours, after which nitrogen (Matheson, less than 5 ppm O_2) was introduced into the heating chamber. The nitrogen was further purified by using a reduced copper catalyst bed (BASF). A slight positive pressure of nitrogen was maintained in the quartz heating tube. After flushing the tube with nitrogen for 2 h at 400°C, the temperature was raised to 760°C for 36 h followed by cooling to 300°C at a rate of 50°C per hour. The furnace power was then shut off, and the furnace and sample were allowed to cool to room temperature. The resulting $(VO)_2P_2O_7$ crystals were grayish in color, having a surface area of 1.00 m^2/g.

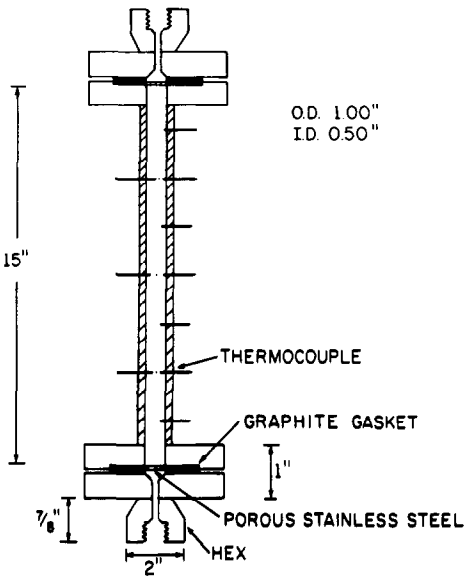

FIG. 1. Integral reactor.

2.B. *Characterization Techniques for Fresh and Used Catalysts*

All phases were examined using X-ray diffraction, laser Raman spectroscopy, Fourier transform infrared spectroscopy, and scanning electron microscopy. Surface areas were also measured.

2.B.1. X-Ray diffraction. X-Ray powder diffraction measurements were made with a Siemans diffractometer with a preset spinning sample mount. CuK_α radiation was used.

2.B.2. Laser Raman spectroscopy. Laser Raman spectra were obtained in the backscattering geometry using a spinning pellet. A Spex 1403 laser Raman spectrometer was used with the 514.3-nm line of a Spectra Physics Model 164 argon ion laser operated at 200 mW at the source. A Nicolet 1180E computer system allowed for spectral accumulation. Raman spectra reported for β-$VOPO_4$ typically represent a five-scan accumulation at 5-cm^{-1} resolution, while those for $(VO)_2P_2O_7$ required as many as twenty scans at the same resolution.

2.B.3. Fourier transform infrared spectroscopy. Infrared spectra were obtained with an IBM IR 98 Fourier transform infrared spectrometer. The instrument was configured for the mid-ir region using KBr windows. Samples were prepared by the KBr disk technique. All spectra represent an accumulation of 100 scans at 4-cm^{-1} resolution.

2.B.4. Scanning electron microscopy. Scanning electron micrographs were obtained using a JEOL Model JSM/U3 scanning electron microscope. Samples were prepared by the gold sputtering technique.

2.B.5. Surface area measurements. Surface areas were measured with a Micromeritics 2100E AccuSorb instrument. Adsorption measurements were performed using krypton as the adsorbate.

2.C. *Catalytic Activity and Selectivity Measurements*

The vapor phase oxidation of n-butane was carried out using an integral flow reactor operating at near atmospheric pressure (Fig. 1). The reactor was constructed from 316 stainless-steel tubing have a 1-in. outer diameter and a $\frac{1}{2}$-in. inner diameter. The overall reactor bed length was 15 in., including the $\frac{1}{2}$-in. thickness of each flange. The temperature along the reactor length

and at varying radial depths was monitored by using 13 subminiature thermocouple probe assemblies (Omega Engineering). These thermocouples yielded information concerning possible axial or radial temperature gradients caused either by "hot spots" or by inadequate heating control. The entire reactor was submerged in a heated fluidized sand bath. Zoned heating of the reactor was also employed by seven independently controlled resistance elements. Typically, the temperature of the catalyst bed could be maintained to within ±2°C. Tylan Model FC260 mass flow controllers were used to regulate flow rates. The feed gas was preheated to near reaction temperature by passage through a coil of $\frac{1}{8}$-in. tubing submerged in the fluidized sand bath.

The reactor was charged with catalyst and No. 8 mesh (2.38 mm) silicon carbide which served as a diluent. The catalyst bed consisted of a homogeneous mixture of 5.00 g of catalyst and 45 g of silicon carbide. Catalyst particles were prepared by pressing disks which were broken and sieved to between Nos. 10 and 20 mesh (1.68 to 0.84 mm).

Exit lines from the reactor were heated to 105°C to prevent maleic anhydride condensation. The composition of both the feed and product gases was analyzed by gas chromatography. The analytical system consisted of an Antex 300 gas chromatograph which was equipped with three heated sampling valves, two flame ionization detectors, and one thermoconductivity detector. The conversion of n-butane was determined by analysis of the feed and product gases. The percentage conversion reported in this work was defined as

$$\frac{\text{moles of n-butane consumed}}{\text{moles of n-butane in feed}} \times 100\%$$

while the percentage selectivity to product N_i was defined as

$$\frac{\text{moles of } N_i \text{ produced}}{\sum 1/\xi_i \text{ (moles of } N_i \text{ produced)}} \times 1/\xi_i \times 100\%,$$

where ξ_i is the ratio of the number of carbon atoms in the reactant to the number of carbon atoms in the product.

A series of experiments was conducted under both steady-state and unsteady-state conditions.

The steady-state kinetic experiments were conducted to examine the effects of contact time (time factor), reaction temperature, and oxygen partial pressure. At least 12 h of reaction occurred before data were collected. The time factor was defined as the ratio W/F, where W is the weight of catalyst (kg) and F is the total molar feed rate (kmol/h at STP). The ranges of operating variables were as follows: partial pressure of oxygen in the feed gas—0.02 to 0.22 atm; reaction temperature—425 to 525°C, time factor—1.2 to 6.2 kg catalyst/kmole/h. The partial pressure of n-butane in the feed gas was held constant at 0.015 atm for all experiments.

Unsteady-state reactor studies were performed to determine the time required to reach steady-state performance. Both the conversion of n-butane and the product distribution were monitored to determine this time period. The partial pressures of oxygen and n-butane in the feed gas were held constant at 0.09 and 0.015 atm, respectively, with a space time of 2.10 kg/kmole/h. At the beginning of these experiments, the packed reactor was flushed with feed gas at room temperature and then lowered into the hot (425°C) fluidized sand bath. The reactor bed was brought to 475°C within 3 h after being submerged in the sand bath using the additional heating provided by the zoned heating elements. Data collection was begun 30 min after the reactor was placed in the sand bath.

2.D. *In Situ Laser Raman Spectroscopy of Functioning Catalysts*

In situ laser Raman spectra of functioning catalysts were obtained using a rotating controlled atmosphere cell similar to the one described by Cheng *et al.* (*18*). Rotation of the sample was useful in avoiding thermal or photochemical decomposition.

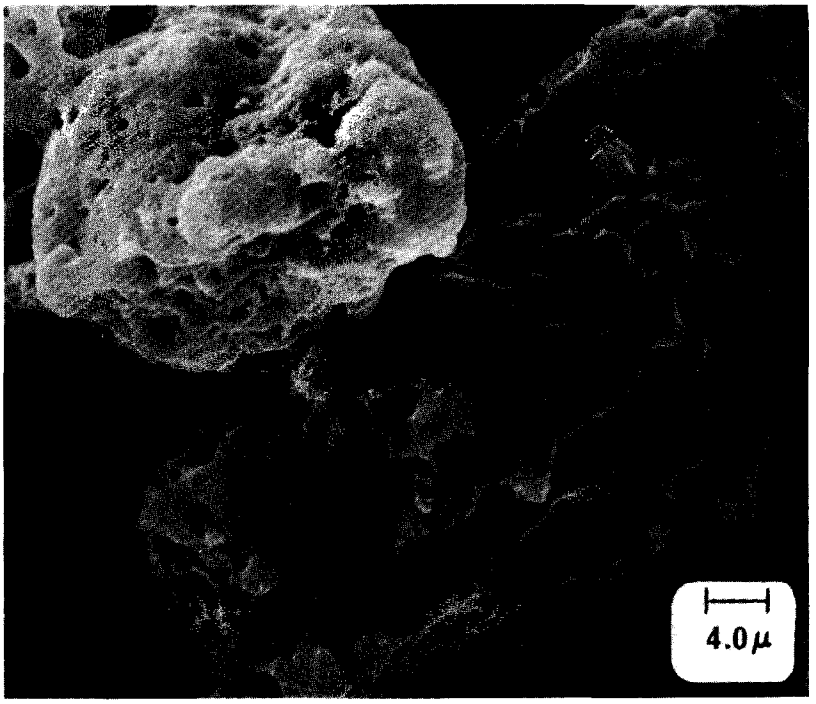

FIG. 2. Scanning electron micrograph of catalyst precursor.

The cell could be heated to near 500°C within the sample compartment of the laser Raman spectrometer. The cell temperature was determined by a thermocouple placed near the pellet holder. The 488.0-nm line of the argon ion laser was used to obtain the Raman spectra with 50 mW of power measured at the source. Typically 10 scans were accumulated at 5-cm^{-1} resolution. Catalyst samples were pressed as pure materials at 17,000 psia into 13-mm-diameter disks. A gas mixture of 0.015 atm n-butane and 0.09 atm oxygen in nitrogen was fed to the cell at 200 cm^3/min. Analysis of the cell effluent gas by gas chromatograph indicated the presence of 1-butene, 2-butenes, 1,3-butadiene, maleic anhydride, and CO_2 as the major reaction products at 475°C.

3. EXPERIMENTAL RESULTS

3.A. Characterization of Fresh Catalysts

The syntheses of both β-$VOPO_4$ and $(VO)_2P_2O_7$ shared a common precursor prepared in oxygen (400°C). The amorphous nature of this precursor has been confirmed by X-ray diffraction and by scanning electron microscopy. (Fig. 2).

3.A.1. β-$VOPO_4$. The X-ray diffraction pattern of β-$VOPO_4$ was compared to that published by both Brown and Hummel (*4*) and Bordes and Courtine (*5*). The *d*-spacings are given in Table 1; excellent agreement between these data and the X-ray pattern published by Brown and Hummel (*4*) is apparent. The absence of one medium intensity line (*d*-spacing at 2.834 Å) in Bordes and Courtine's (*5*) X-ray results is likely an inadvertent omission. Scanning electron microscopy confirmed that a crystalline material was present. The β-$VOPO_4$ phase formed crystalline sheets in the range of 2 to 5 μm (Fig. 3).

The infrared spectrum of β-$VOPO_4$ (Fig. 4) was compared to that of Bhargava and Condrate (*8*) and Bordes and Courtine (*5*). The band assignments discussed here are in agreement with those given by these au-

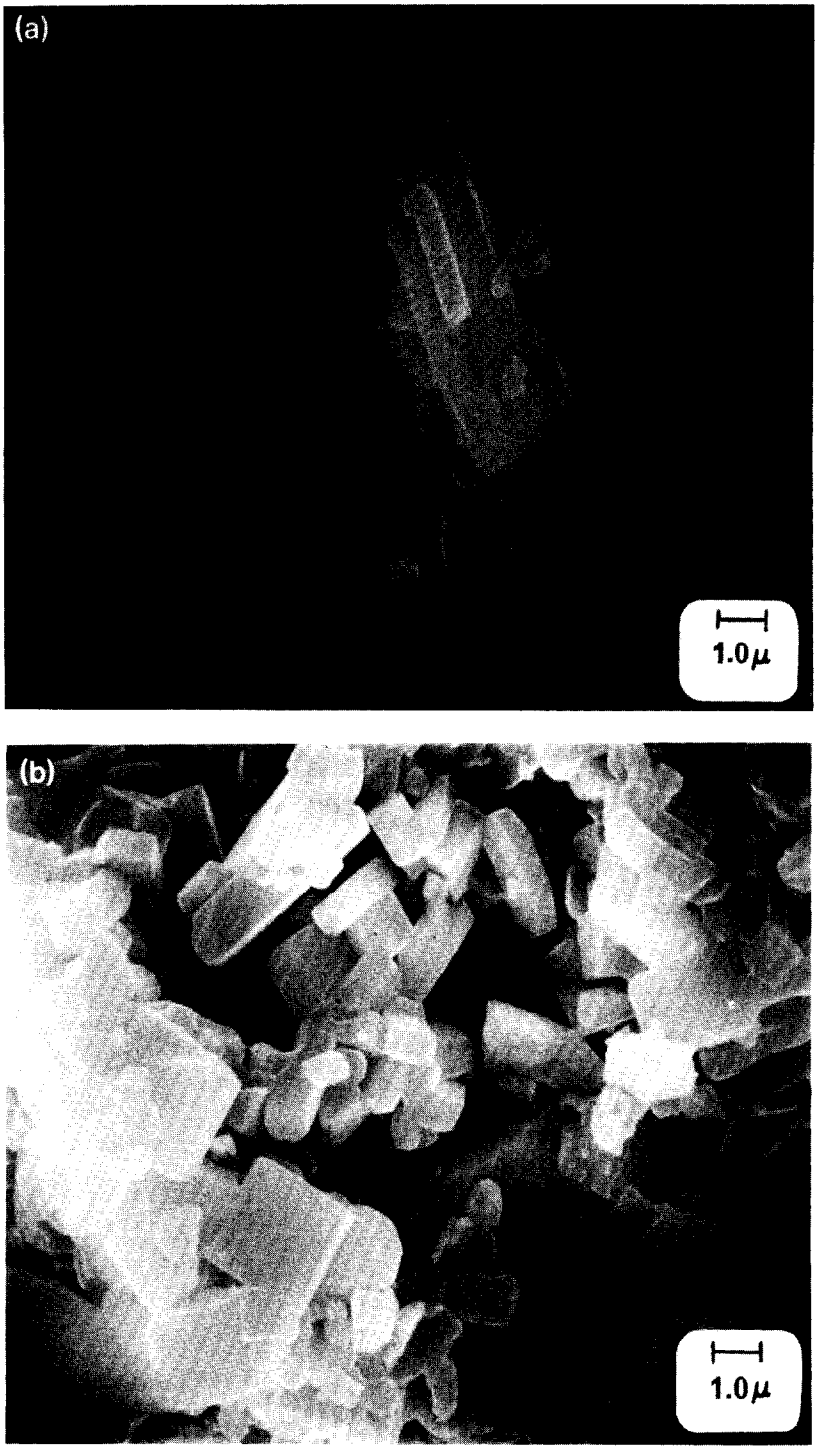

FIG. 3. Scanning electron micrographs of model catalysts. (a) β-$VOPO_4$ and (b) $(VO)_2P_2O_7$.

TABLE 1

X-Ray Diffraction Patterns of Model V–P–O Catalysts

β-$VOPO_4$		$(VO)_2P_2O_7$	
d-Spacing, Å	Relative intensity	*d*-Spacing, Å	Relative intensity
5.233	(31.6)	6.323	(14.4)
4.629	(31.5)	5.707	(14.7)
3.985	(11.0)	4.826	(13.9)
3.903	(23.6)	4.090	(6.2)
3.501	(23.4)	3.889	(100.0)
3.416	(100.0)	3.147	(88.8)
3.196	(24.9)	2.991	(49.0)
3.078	(50.9)	2.921	(7.5)
2.983	(22.2)	2.662	(20.8)
2.834	(13.7)	2.444	(20.6)
2.648	(12.6)	2.363	(9.4)
2.607	(8.0)	2.256	(6.6)
2.415	(6.1)	2.095	(29.7)
2.281	(7.5)	1.994	(8.6)
2.213	(10.5)	1.937	(10.5)
2.178	(9.5)	1.842	(16.8)
2.092	(7.6)	1.796	(6.1)
2.000	(7.7)	1.648	(6.3)
1.986	(5.3)	1.577	(19.1)
1.965	(14.9)	1.475	(8.4)
1.751	(7.6)	1.460	(10.7)
1.726	(7.5)		
1.703	(6.9)		
1.641	(8.6)		
1.607	(12.7)		
1.538	(30.9)		

thors. Group factor analysis for β-$VOPO_4$ predicts 31 bands (*8*) for the infrared spectrum: in this research, 12 bands (Table 2) have been observed, although the band structure is quite complex. Some uncertainty remains about the actual wavenumber position of the V=O stretch. In V_2O_5, the stretching frquency of the V=O group is at 1018 cm^{-1}, while the stretching frequency of the V—O—V group is at 820 cm^{-1} (*19*). This would suggest that the strong band in the infrared at 1001 cm^{-1} is due to the V=O stretch. The stretching vibration of P—O—P occurs in the region 870 to 1000 cm^{-1} for inorganic phosphorus compounds (*20*). Thus, the band at 951 cm^{-1} can be attributed to P–O stretching.

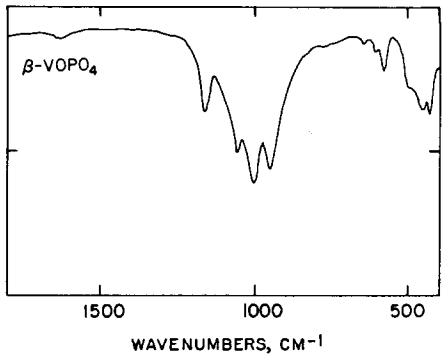

FIG. 4. Infrared spectrum of β-$VOPO_4$.

The bands at 1055 and 1163 cm^{-1} are probably ionic P–O stretches. The positions of these ionic phosphate bands may reflect variations in the P–O bond lengths.

Group factor analysis predicts that 42 bands are Raman active for β-$VOPO_4$ (*8*). A total of 22 bands are reported for the region 100 to 1200 cm^{-1} (Fig. 5); corresponding wavenumber positions are given in Table 3. The assignments discussed here are in agreement with those of Bhargava and Condrate (*8*), although weak bands at 738, 775, and 801 cm^{-1} were not observed by these

TABLE 2

Infrared Spectra of Model V–P–O Catalysts (cm^{-1})

	1500–1001	1000–501	500–0
β-$VOPO_4$	1163 s	951 s	500 m
	1055 s	777 vw	453 m
	1001 vs	737 vw	430 m
		644 vw	
		608 w	
		581 m	
$(VO)_2P_2O_7$	1267 s	991 s	442 s
	1254 s	941 vs	430 s
	1221 m	928 s	
	1203 w	827 vw	
	1186 m	798 w	
	1167 w	746 m	
	1151 vs	665 vw	
	1130 m	637 m	
	1121 w	621 w	
	1063 s	561 s	
	1011 w	515 m	

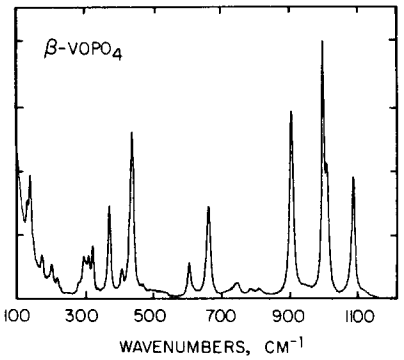

FIG. 5. Raman spectrum of β-$VOPO_4$.

authors. The V=O stretching frequency for V_2O_5 is at 994 cm^{-1} in the Raman spectrum (*19*), suggesting that the band at 997 cm^{-1} of β-$VOPO_4$ can be assigned to this mode. The bands at 655, 895, 985, and 1073 cm^{-1} can be assigned to P–O stretching and bending of the PO_4 units—both symmetric and asymmetric modes (*20*). The bands from 280 to 475 cm^{-1} are assigned to coupled V–O and P–O bending vibrations, whereas those below 280 cm^{-1} are a result of the skeletal vibration of VO_6 and PO_4 groups.

TABLE 3

Raman Spectra of Model V–P–O Catalysts (cm^{-1})

	0–300	301–600	601–900	900+
β-$VOPO_4$	131 w	308 m	655 s	985 vs
	140 m	321 m	738 vw	997 s
	175 m	368 s	775 vw	1073 s
	203 m	405 m	801 vw	
	217 w	434 vs	895 vs	
	280 w	463 w		
	295 m	598 m		
$(VO)_2P_2O_7$	255 w	309 w	802 vw	923 vs
	274 w	336 w		934 s
		372 w		963 w
		392 w		1003 vw
		411 vw		1023 vw
		457 vw		1051 vw
		491 vw		1128 w
				1140 w
				1168 vw
				1187 m
				1199 w

3.A.2. $(VO)_2P_2O_7$. The *d*-spacings for $(VO)_2P_2O_7$ are given in Table 1, showing agreement with that reported previously (*5*). The most intense characteristic diffraction lines of $(VO)_2P_2O_7$ have spacings of 2.991, 3.147, and 3.889 Å. Scanning electron microscopy also confirmed the high crystallinity of the $(VO)_2P_2O_7$ preparation. $(VO)_2P_2O_7$ existed as crystalline particles in the range of 1 to 4 μm (Fig. 3).

The infrared spectrum of $(VO)_2P_2O_7$ is given in Fig. 6, with corresponding wavenumber positions listed in Table 2. The infrared spectrum clearly indicates the presence of the $P_2O_7^{4-}$ anion. For the infrared spectrum of tetrasodium pyrophosphate ($Na_4P_2O_7$), P–O–P stretching vibrations have been detected in ranges from 714 to 730 cm^{-1} (symmetric) and from 900 to 915 cm^{-1} (asymmetric); PO_3 stretching vibrations have been observed in spectral regions from 1100 to 1150 cm^{-1} (asymmetric) and from 1016 to 1030 cm^{-1} (symmetric). Other assignments for the pyrophosphate ion are given by Greenfield and Clift (*21*). The bands between 1121 to 1186 cm^{-1} can be assigned to the asymmetric stretches of the PO_3 group, while the bands at 928 and 941 cm^{-1} are assigned to the asymmetric P–O–P stretches. The V=O stretch is identified with the absorption at 991 cm^{-1}, which is in the same spec-

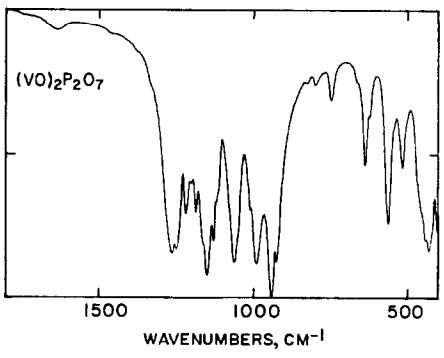

FIG. 6. Infrared spectrum of $(VO)_2P_2O_7$.

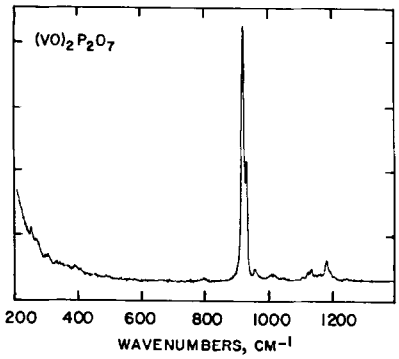

FIG. 7. Raman spectrum of $(VO)_2P_2O_7$.

tral region as the V=O assignment for β-$VOPO_4$, α-$VOPO_4$, and V_2O_5.

The Raman spectrum of $(VO)_2P_2O_7$ is shown in Fig. 7 with wavenumber positions provided in Table 3. The spectral data has not been previously reported in the literature; however, the Raman technique proved to be a very sensitive probe for the presence of $VOPO_4$-like impurities. The strong bands at 923 and 934 cm^{-1} are assigned to P–O–P asymmetric stretches of the pyrophosphate ion. The spectral region between 960 to 1025 cm^{-1} showed a number of weak bands (963, 1003, and 1023 cm^{-1}). The V=O stretch is probably at 963 cm^{-1} while the bands at 1003 and 1023 cm^{-1} are PO_3 stretches. The strong bonding of the pyrophosphate ion are reflected in the high-frequency, weak bands at 1128, 1140, 1187, and 1199 cm^{-1}.

3.B. Catalyst Activity and Selectivity for n-Butane Oxidation under Steady-State Conditions

Three parameters were varied to investigate their effect on catalyst activity and selectivity: time factor, temperature, and oxygen partial pressure.

3.B.1. Effect of time factor. Figures 8a and b show the relationships between conversion or selectivity and the time factor *W/*

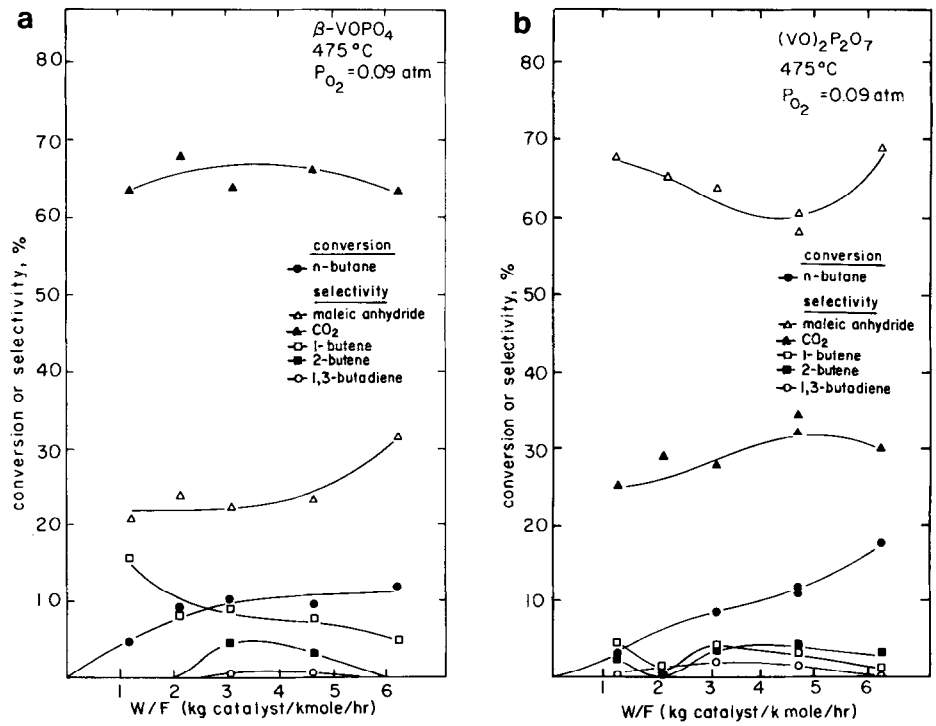

FIG. 8. Selective oxidation of n-butane over (a) β-$VOPO_4$ and (b) $(VO)_2P_2O_7$, as a function of time factor.

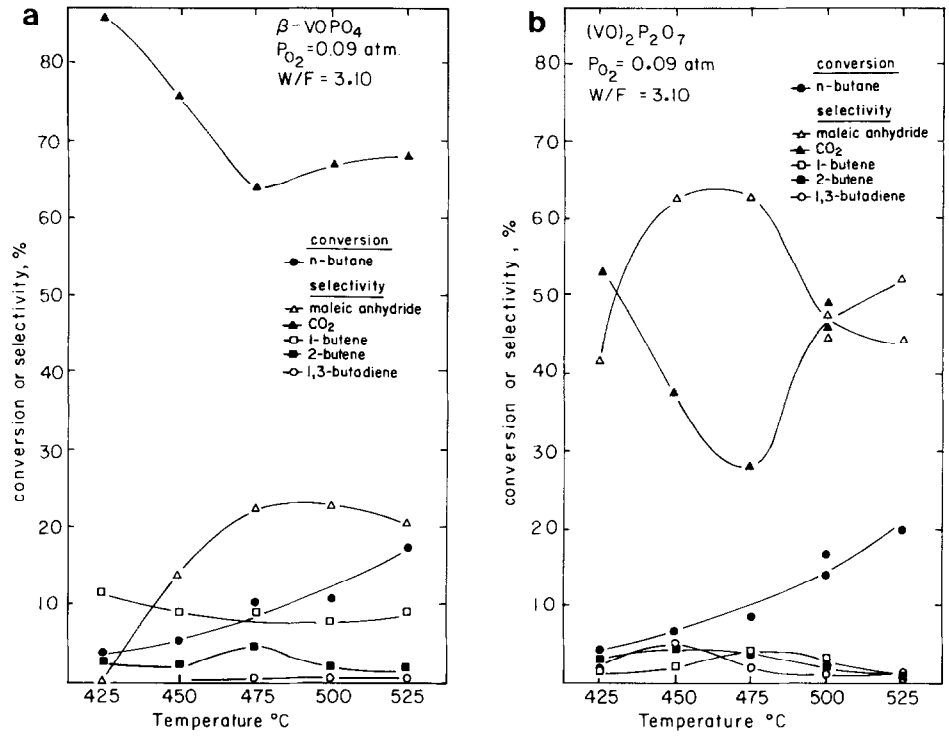

FIG. 9. Selective oxidation of n-butane over (a) β-$VOPO_4$ and (b) $(VO)_2P_2O_7$, as a function of temperature.

F for β-$VOPO_4$ and $(VO)_2P_2O_7$ at 475°C, respectively.

For β-$VOPO_4$ the selectivity to maleic anhydride increased gradually with increasing W/F (Fig. 8a). The production of 1-butene was highest at small time factors, decreasing with increasing W/F. Smaller amounts of 2-butenes and 1,3-butadiene were also observed in the product effluent. The conversion of n-butane monotonically increased with increasing W/F.

For n-butane oxidation by $(VO)_2P_2O_7$, a broad minimum in selectivity to maleic anhydride was observed, with a simultaneous occurrence of a maximum in selectivity to carbon dioxide (Fig. 8b). Small amounts of 1-butene, 2-butenes, and 1,3-butadiene were detected in the product effluent. For larger W/F values, the conversion of n-butane steadily increased.

3.B.2. Effect of temperature. The effect of temperature on the activity and selectivity of β-$VOPO_4$ and $(VO)_2P_2O_7$ is shown in Fig. 9.

For β-$VOPO_4$ a maximum in selectivity for maleic anhydride formation was observed between 475 and 500°C. Production of maleic anhydride was very low at 425°C. A broad minimum in 1-butene selectivity was observed, approximately corresponding to the maximum in maleic anhydride selectivity. Conversely, a maximum in selectivity to 2-butenes was observed in this temperature range. The production of carbon dioxide decreased as the conversion to maleic anhydride increased. Above 475°C trace amounts of 1,3-butadiene were also detectable. The conversion of n-butane gradually increased with increasing temperature.

The activity and selectivity of the $(VO)_2P_2O_7$ catalyst phase as a function of temperature was also investigated. Figure 9 shows the results of n-butane oxidation be-

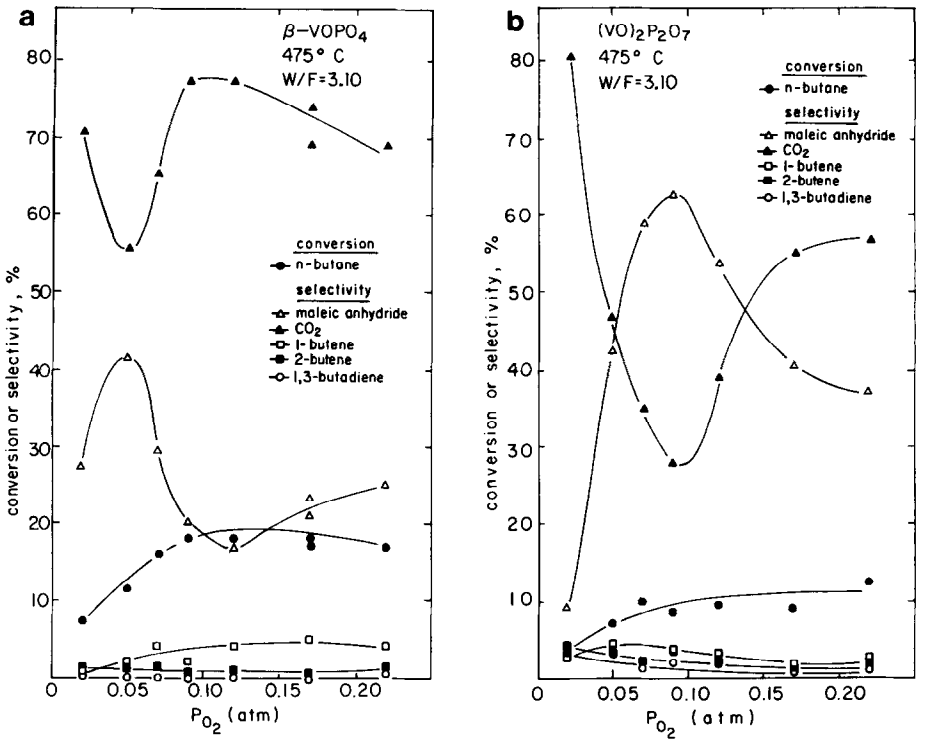

FIG. 10. Selective oxidation of n-butane over (a) β-$VOPO_4$ and (b) $(VO)_2P_2O_7$, as a function of oxygen partial pressure.

tween 425 and 525°C. A maximum in maleic anhydride selectivity occurred between 450 and 475°C, while the carbon dioxide selectivity followed an opposite relationship and had a minimum near 475°C. The selectivity to 2-butenes and 1,3-butadiene passed through a maximum near 450°C, while a maximum in 1-butene selectivity occurred at 475°C. The conversion of n-butane increased monotonically with temperature.

3.B.3. Effect of oxygen partial pressure. Figure 10 shows the selective oxidation of n-butane by β-$VOPO_4$ and $(VO)_2P_2O_7$ as a function of oxygen partial pressure at 475°C.

For β-$VOPO_4$ a maximum in selectivity to maleic anhydride was noted at a low partial pressure of oxygen (0.05 atm), while a less prominent minimum in selectivity to maleic anhydride occurred at an intermediate partial pressure of oxygen (0.12 atm). The selectivity to carbon dioxide followed an opposite trend, showing a minimum selectivity at 0.05 atm and a maximum selectivity at 0.12 atm. The β-$VOPO_4$ phase produced only small amounts of 1,3-butadiene over the entire range of oxygen partial pressures. The selectivity to 2-butenes remained constant at about 1 to 2%, while the selectivity to 1-butene gradually increased with the partial pressure of oxygen. The conversion of n-butane remained constant for partial pressures of oxygen greater than 0.09 atm; the activity decreased sharply for lower oxygen partial pressures.

Figure 10 shows the selective oxidation of n-butane at 475°C as a function of oxygen partial pressure using $(VO)_2P_2O_7$. A maximum in maleic anhydride selectivity was observed at an oxygen partial pressure of 0.09 atm. For lower oxygen partial pressures, the selectivity to maleic anhydride decreased, as did the activity. The minimum in carbon dioxide selectivity was co-

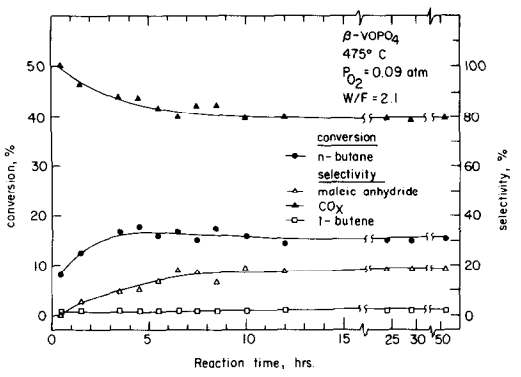

FIG. 11. On-line approach to steady-state operation for β-$VOPO_4$.

incident with the maximum in maleic anhydride selectivity. As shown in Fig. 10, 1-butene selectivity went through a maximum at an oxygen partial pressure of 0.05 atm—the region where the selectivity to maleic anhydride also increased most rapidly. A small decrease in selectivity to other dehydrogenation products such as 2-butenes and 1,3-butadiene was apparent as the oxygen partial pressure increased.

3.C. *Unsteady-State Reactor Studies*

Figures 11 and 12 show the catalytic activity of β-$VOPO_4$ and $(VO)_2P_2O_7$, respectively, as a function of time on stream; the final temperature of the reactor system was 475°C (achieved after 3 h).

The β-$VOPO_4$ phase initially exhibited a lower selectivity to maleic anhydride compared to that achieved after steady-state operation was reached (Fig. 11). The selectivity to maleic increased from near 0% after 30 min on-stream to the steady-state value of about 20% after 6 h. The selectivity to 1-butene remained roughly constant (1 to 2%) while lesser amounts of 2-butenes and 1,3-butadiene were detected. A small amount of CO was also detected in the product effluent.

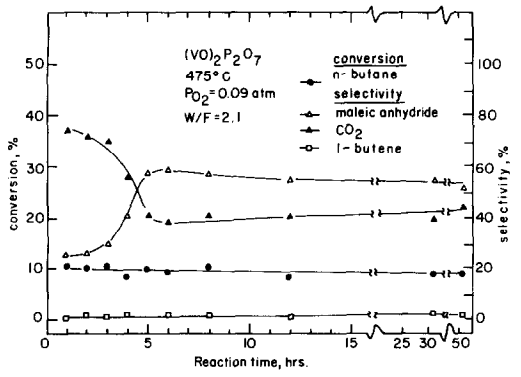

FIG. 12. On-line approach to steady-state operation for $(VO)_2P_2O_7$.

The $(VO)_2P_2O_7$ phase reached steady conditions after about 5 h on stream (Fig. 12). The initial selectivity to maleic anhydride (after 1 h) was about 25% and gradually increased to the steady value of about 57%. The selectivity to 1-butene remained constant (1 to 2%). Only small amounts of 2-butenes and 1,3-butadiene were produced (not indicated in Fig. 12).

3.D. *Raman Spectra of Catalysts at Hydrocarbon Oxidation Conditions*

In situ Raman spectra for both β-$VOPO_4$ and $(VO)_2P_2O_7$ are given in Figs. 13 and 14,

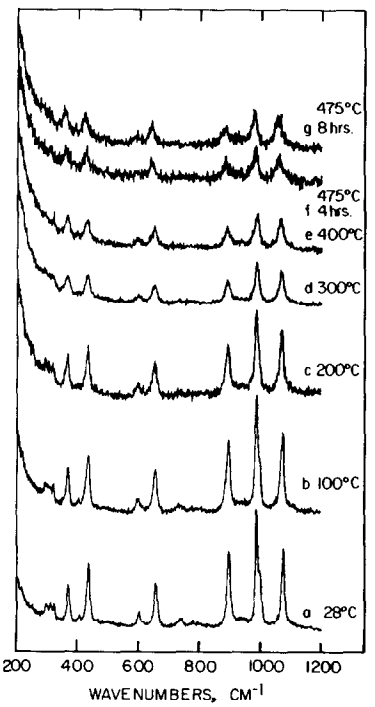

FIG. 13. *In situ* Raman spectra of β-$VOPO_4$.

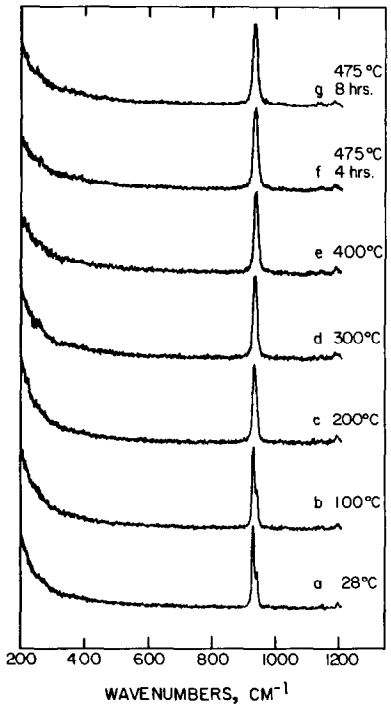

FIG. 14. *In situ* Raman spectra of $(VO)_2P_2O_7$.

respectively, for temperatures from 28 to 475°C under reaction conditions. All bands characteristic of the fresh catalysts (pure compounds) were observed at elevated temperatures. No development of new bands was detected. The Raman spectra of active catalysts exposed to reactive hydrocarbon–air mixtures at 475°C for 4 to 8 h also exhibited bands which were characteristic of the initial materials.

4. DISCUSSION OF RESULTS

4.A. Syntheses of Pure Model Catalysts

The syntheses of both β-$VOPO_4$ and $(VO)_2P_2O_7$ proved to be sensitive to the preparation procedures used during calcination or reduction. Factors such as cooling rate, oxygen partial pressure in the flowing gas, and homogenization of the solid precursors were all recognized as being important factors in the catalyst preparation.

The synthesis of β-$VOPO_4$ was complicated by the formation of polycondensed phosphates. A slow cooling rates was critical in obtaining β-$VOPO_4$ crystals free of condensed phosphates. A cooling rate of 40°C per hour or slower was found to be sufficient, following calcination at 600°C. Other researchers have also observed the formation of polycondensed phosphates. Martini *et al.* (*14*) found that V–P–O catalysts with P/V ratios greater than 1.1 contained polycondensed phosphates which were identified as pyrophosphates and metaphosphates. Their infrared spectra showed a continuous increase in absorption for the region 1260 to 1280 cm^{-1} as the P/V ratio was increased from 1.0 to 1.8. A similar experiment was conducted as a part of our research involving the solid-state synthesis of β-$VOPO_4$. Figure 15 shows the infrared spectra of material prepared with P/V ratios ranging from 0.7 to 2.0. These compounds were allowed to cool to room temperature in the furnace by turning off the power at 600°C. This rapid cooling rate allowed the formation of polycondensed phosphates structures, even for P/V ratios as low as 0.7. The characteristic polycon-

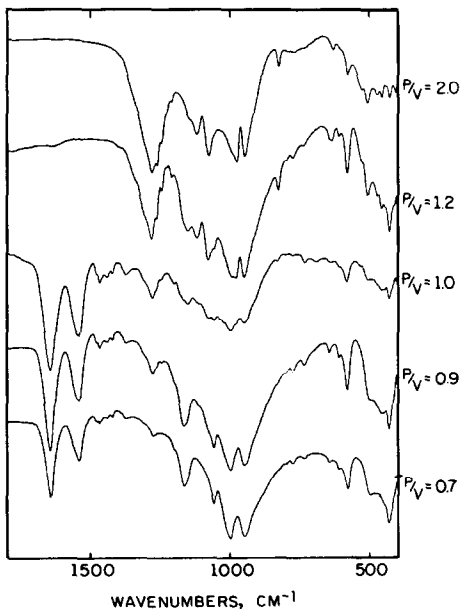

FIG. 15. Infrared spectra of V–P–O compounds with various P/V atomic ratios.

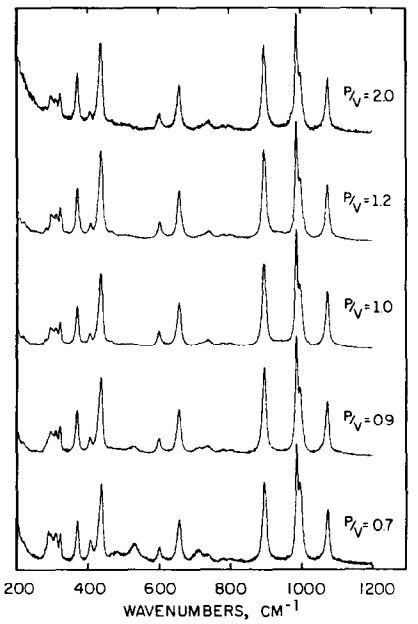

FIG. 16. Raman spectra of V–P–O compounds with various P/V atomic ratios.

densed phosphate absorbance in the region 1200 to 1280 cm^{-1} continuously increased with greater phosphorus loadings. The presence of the bands at 1538 and 1640 cm^{-1} for low phosphorus compounds (P/V < 1.2) indicated the existence of surface O–H stretching and bending vibrations associated with waters of crystallization.

It is likely that the condensed phosphates exist both as long-chain linear phosphates and metaphosphates. The infrared spectrum for P/V = 2.0 (Fig. 15) compares closely with the spectrum of $VO(PO_3)_2$ (*5*) whose structure is based on metaphosphate groups. Long-chain linear phosphates are known to have PO_2 stretches (asymmetric) from 1200 to 1300 cm^{-1} and from 1100 to 1170 cm^{-1}; P–O–P stretches are observed from 850 to 1050 cm^{-1} (asymmetric) and from 650 to 800 cm^{-1} (symmetric). The infrared spectra of metaphosphate compounds show similar strong absorptions in the region 1205 to 1315 cm^{-1} (P–O–P ring stretches).

Raman spectroscopy was used to detect unreacted V_2O_5 for P/V ratios less than 1.0 (indicated by a weak band at 529 cm^{-1} in Fig. 16). The presence of unreacted V_2O_5 was also confirmed by X-ray diffraction using the characteristic *d*-spacings of V_2O_5 (2.89, 4.38, and 5.78 Å). These X-ray patterns also indicated that the crystallinity of V–P–O compounds decreased as the P/V ratio increased, possibly a result of the amorphous nature of condensed phosphate structures.

The preparation of $(VO)_2P_2O_7$ by the solid-state technique was also very sensitive to synthesis treatments. Reduction of β-$VOPO_4$ (*5*) to obtain pure $(VO)_2P_2O_7$ crystals was not successful using either nitrogen or hydrogen; the direct heating of V_2O_5 and $NH_4H_2PO_4$ in nitrogen (*5*) was similarly ineffective. The reduction of β-$VOPO_4$ in nitrogen produced a mixture of phases including β-$VOPO_4$, $(VO)_2P_2O_7$, and a phase referred to as α_{II}-$VOPO_4$ (*22*) (characteristic *d*-spacing at 3.57 Å). The direct heating of V_2O_5 and $NH_4H_2PO_4$ (P/V = 1.00) in nitrogen (P_{O_2} < 5 ppm) produced a grayish material. X-Ray diffraction indicated that this material was amorphous.

$(VO)_2P_2O_7$ crystals were successfully prepared by a two-step process: calcination of a mixture of V_2O_5 and $NH_4H_2PO_4$ in oxygen (400°C) followed by heating in nitrogen (760°C). Both scanning electron microscopy (see Fig. 2) and X-ray diffraction indicated that the precursor prepared in oxygen was amorphous. The preparation of the precursor and the very low oxygen partial pressure in the reducing (nitrogen) atmosphere proved to be the critical preparative parameters for this preparative route.

4.B. Reaction Pathway Products

Relatively simple reaction pathways have been suggested for the conversion of n-butane to maleic anhydride. For V–P–O catalysts, Wohlfahrt and Hofmann (*16*) and Escardino *et al.* (*17*) proposed conversion of n-butane to maleic anhydride or CO_2 and H_2O; combustion of maleic anhydride was also included in the kinetic scheme. Forma-

tion of dehydrogenated or other partially oxidized hydrocarbons was not reported. Other studies have also not indicated the formation of these side products under realistic reactor operating conditions. However, in our work, considerable amounts of butenes and butadiene were formed. Previous studies of 1-butene oxidation using V–P–O catalysts have proposed that these species are intermediates in the pathway for maleic anhydride production. Our studies of n-butane (paraffin) oxidation also have shown that these compounds are produced at typical industrial operating conditions involving low hydrocarbon concentrations in air; high selectivities to maleic anhydride were observed concurrently. Therefore, it is not possible to exclude butenes and butadiene as possible reaction pathway intermediates for n-butane oxidation. Studies of n-butane oxidation involving other catalysts such as cobalt molybdate (*23*) and Co–Mo–O or V–Mo–O (*24*) have indicated butenes as reaction pathway intermediates.

Several other aspects of the reactor studies should be noted. Further oxidation of maleic anhydride to carbon dioxide apparently became significant for temperatures above 475°C. A pronounced decrease in maleic anhydride selectivity and a corresponding increase in carbon dioxide production were observed for temperatures above 475°C for both the β-$VOPO_4$ and $(VO)_2P_2O_7$ phases (Fig. 9). No CO formation was observed in these studies. For the selective oxidation of 1-butene to maleic anhydride over V–P–O catalysts, Cavani *et al.* (*25*) observed only carbon dioxide at low conversions, while both carbon monoxide and dioxide were detected at high conversions.

The unsteady-state experiments indicated that 5 to 6 h of reaction time was necessary to reach steady-state performance. The approach to steady conditions is partially affected by the time (approximately 3 h) to bring the reactor to 475°C.

4.C. Stability of β-$VOPO_4$ and $(VO)_2P_2O_7$ Catalysts

In situ laser Raman spectra recorded between 28 and 475°C indicated that the β-$VOPO_4$ and $(VO)_2P_2O_7$ structures were remarkably stable for several hours under reaction conditions at high temperature. Previous (*26*) post-catalytic characterization by X-ray diffraction has suggested that a phase transition occurs for β-$VOPO_4$ in n-butane oxidation. A mixture of β-$VOPO_4$ and α-$VOPO_4$ was believed to form. In our work, it was determined by *in situ* Raman spectroscopy and by post-catalytic characterization using X-ray diffraction and infrared spectroscopy that no phase transitions had occurred for either β-$VOPO_4$ or $(VO)_2P_2O_7$. No α-$VOPO_4$ formation was observed for any samples.

However, comparison of the absolute intensities (photon counts/sec) of the Raman bands did indicate some alteration of the catalyst state. Under reaction conditions, the intensities of the β-$VOPO_4$ bands decreased by a factor of 3 over the temperature range 28 to 475°C. This change is relatively modest. The Raman spectra clearly indicate that β-$VOPO_4$ is present even at the highest temperatures. The modifications in the Raman spectra for this phase would seem to imply that some reduction occurs, but not throughout the catalyst structure. Changes in intensities of the Raman bands for the $(VO)_2P_2O_7$ phase appear to be less significant. A small decrease in the absolute intensities of the Raman bands occurs at higher temperatures. Some uncertainty exists in the absolute values for the intensities measured in these experiments because of changes in sample alignment which occur as the temperature is increased. Additional investigations involving *in situ* Raman spectroscopy will be reported elsewhere (*27*).

ACKNOWLEDGMENTS

This work was conducted through the Ames Laboratory which is operated for the U.S. Department of

Energy by Iowa State University under Contract W-7405-Eng-82. This research was supported by the Office of Basic Energy Sciences, Chemical Sciences Division. The scanning electron microscopy work done by David Bohlen is gratefully acknowledged.

REFERENCES

1. Malow, M., *Hydrocarbon Process.*, 149 (1980).
2. Mount, R. A., "Encyclopedia of Chemical Technology," Vol. 14, 3rd ed. Wiley, New York, 1981.
3. Varma, R. L., and Saraf, D. N., *Ind. Eng. Chem. Prod. Res. Dev.* **18**(1), 7 (1979).
4. Brown, J. J., and Hummel, F. A., *Trans. Br. Ceram. Soc.* **64,** 419 (1965).
5. Bordes, E., and Courtine, P., *J. Catal.* **57,** 236 (1979).
6. Bordes, E., Courtine, P., and Pannetier, G., *Ann. Chim.* **8**(2), 105 (1973).
7. Gopal, R., and Calvo, C., *J. Solid State Chem.* **5,** 432 (1972).
8. Bhargava, R. N., and Condrate, R. A., *Appl. Spectrosc.* **31**(3), 230 (1977).
9. Hodnett, B. K., Permanne, Ph., and Delmon, B., *Appl. Catal.* **6,** 231 (1983).
10. Morselli, L., Trifirò, F., and Urban, L., *J. Catal.* **75,** 112 (1982).
11. Poli, G., Resta, I., Ruggeri, O., and Trifirò, F., *Appl. Catal.* **1,** 395 (1981).
12. Morselli, L., Riva, A., Trifirò, F., Zucchi, M., and Emig, G., *Chim. Ind.* **60**(10), 791 (1978).
13. Wüstneck, N., Wolf, H., and Seeboth, H., *React. Kinet. Catal. Lett.* **21**(4), 497 (1982).
14. Martini, G., Vaccari, A., and Trifiró, F., *J. Phys. Chem.* **86,** 1573 (1982).
15. Nakamura, M., Kawai, K., and Fujiwara, Y., *J. Catal.* **34,** 345 (1974).
16. Wohlfahrt, K., and Hofmann, H., *Chem. Ing. Tech.* **52**(10), 811 (1980).
17. Escardino, A., Solá, C., and Ruiz, F., *An. Quim.* **69,** 385 (1973).
18. Cheng, C. P., Ludowise, J. D., and Schrader, G. L., *Appl. Spectrosc.* **34**(2), 146 (1980).
19. Sanchez, C., Livage, J., and Lucazeau, G., *J. Raman Spectrosc.* **12**(1), 68 (1982).
20. Corbridge, D. E. C., and Lowe, E. J., *J. Chem. Soc.*, 4555 (1954).
21. Greenfield, S., and Clift, M., "Analytical Chemistry of the Condensed Phosphates." Pergamon, Oxford, 1975.
22. Tachez, M., Theobald, F., and Bordes, E., *J. Solid State Chem.* **40,** 280 (1981).
23. Bissot, T. C., and Benson, K. A., *Ind. Eng. Chem. Prod. Res. Dev.* **2,** 57 (1963).
24. Agasiev, R. A., Ioffe, I. I., Shakhtakhtinskii, T. N., Sadykhova, Kh. I., and Alieva, K. Ya., *Azerb. Khim. Zh.* **4,** 60 (1969).
25. Cavani, F., Centi, G., Manenti, I., Riva, A., and Trifiró, F., *Ind. Eng. Chem. Prod. Res. Dev.* **22,** 565 (1983).
26. Matsuura, I., "Proceedings, 8th International Congress on Catalysis in Berlin," Vol. IV., p. 473 (1984).
27. Moser, T. P., and Schrader, G. L., to be submitted for publication.